Nuclear Materials and Energy 24 (2020) 100768

Contents lists available at ScienceDirect

Nuclear Materials and Energy

journal homepage: www.elsevier.com/locate/nme

# Dynamic constitutive relationship of CuCrZr alloy based on Johnson-Cook model

Xinyuan Qian[a,b], Xuebing Peng[c], Yuntao Song[c,*], Jianjun Huang[a], Yanpeng Wei[d], Peng Liu[c], Xin Mao[c], Jianwu Zhang[e], Liang Wang[c]

[a] College of Physics and Optoelectronic Engineering, Shenzhen University, Shenzhen 518060, China
[b] Advanced Energy Research Center, Shenzhen University, Shenzhen 518060, China
[c] Institute of Plasma Physics, Chinese Academy of Sciences, Hefei 230031, China
[d] Key Laboratory of Mechanics in Fluid Solid Coupling Systems, Institute of Mechanics, Chinese Academy of Sciences, Beijing 100190, China
[e] Department of Engineering and Applied Physics, School of Physical Sciences, University of Science and Technology of China, Hefei 230026, China

ARTICLE INFO

*Keywords:*
CuCrZr alloy
Johnson-Cook model
Dynamic compressive behavior
Plasma facing components

ABSTRACT

CuCrZr alloy has been acknowledged as one of the most promising candidate materials for the heat sink of plasma facing components in nuclear fusion devices with its excellent thermal conductivity and specific mechanical strength. For the safety concern, it is vital to provide appropriate safety assessment on these mechanical structures with CuCrZr alloy, such as divertor and blanket, under high strain rate loading conditions like displacement events, disruption, and so on. In this work, the dynamic compressive behavior of the CuCrZr alloy over wide range of strain rates and temperatures was investigated using the split Hopkinson pressure bar technique. Based on the experiment results, a constitutive equation is built by using Johnson-Cook model to describe the dynamical property of CuCrZr alloy. However, the results indicated that the influences of the strain, strain rate and temperature on the dynamic behavior are not independent. Therefore, a modified Johnson-Cook model was further developed to take the coupled effects of strain, strain rate and temperature into account. Compared with the original Johnson-Cook model, the modified Johnson-Cook model calculated results show good agreement with the experimental data.

## 1. Introduction

Owing to its excellent properties, CuCrZr alloy is considered as an attractive material in the fusion devices such as ITER and DEMO [1–5]. Especially, it had already been applied as heat sink material for the water-cooled plasma facing components (PFC) in EAST, JET, W-7X [6–8], and so on. In the fusion devices, the PFC structures need to endure different type of loads caused by pulsed plasma operation and off-normal events (e.g. vertical displacement events, disruption, and so on). In this complex circumstance, it is necessary to ensure that all the PFC structures can meet the design requirements.

Considering that most of the off-normal events will generate transient loads in the PFC structures, then doing the analysis of the dynamic response characteristics of the structures during these events allows a better understanding of the behavior of the PFC structures in the fusion device. In order to make an assessment of the possible structural response behavior by computational analysis, the dynamic constitutive relationship of the materials is needed.

In our previous work, the dynamical mechanical property of tungsten was studied [9]. The aim of this paper is to provide the material parameters for CuCrZr alloy in terms of the Johnson-Cook model considering the effects of strain hardening, strain rate hardening and temperature softening [10]. To this end, experiments on CuCrZr alloy over wide range of strain rates (500–2200 $s^{-1}$) and temperatures (20–600 °C) were investigated by using the split Hopkinson pressure bar (SHPB) technique. The rest of this paper is organised as follows. In section 2, descriptions of the theoretical background for SHPB technique and Johnson-Cook model were given. And the experiment setup and results were presented in section 3 and section 4, respectively. Then, the constitutive equations of Johnson-Cook model and modified Johnson-Cook model for CuCrZr alloy were built in section 5. Finally, general conclusions were drawn in section 6.

* Corresponding author.
*E-mail address:* songyt@ipp.ac.cn (Y. Song).

https://doi.org/10.1016/j.nme.2020.100768
Received 11 February 2020; Received in revised form 18 June 2020; Accepted 19 June 2020
Available online 27 June 2020

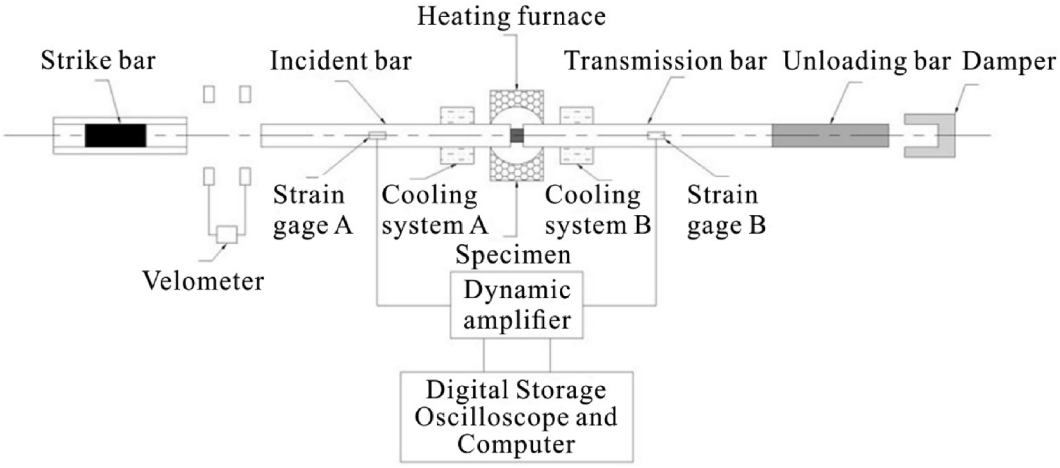


**Fig. 1.** The schematic of the Split Hopkinson Pressure Bar.

## 2. Theoretical background

### 2.1. SHPB technique

The SHPB technique was proposed by Hopkinson and developed by Kolsky. And it is widely used to measure the material dynamic mechanical properties [11]. The schematic diagram of the experiment is shown in Fig. 1 [9].

The basic idea of the SHPB is that the specimen is deformed between two bars excited above their resonant frequency. The raw data of the incident pulse $\varepsilon_i(t)$, transmitted pulse $\varepsilon_t(t)$ and reflected pulse $\varepsilon_r(t)$ are recorded by the strain gauges, respectively, as shown in Fig. 2. The relationship of these parameters is

$$\varepsilon_i(t) = \varepsilon_t(t) - \varepsilon_r(t) \tag{1}$$

According to one-dimensional stress wave theory, the dynamic mechanical parameters of specimens could be calculated indirectly by the recorded data in the strain gauges. The stress $\sigma(t)$, strain $\varepsilon(t)$ and strain rate $\dot{\varepsilon}(t)$ can be expressed as follows:

$$\sigma(t) = \frac{EA}{2A_s}[\varepsilon_i(t) + \varepsilon_r(t) + \varepsilon_t(t)] \tag{2}$$

$$\varepsilon(t) = \frac{c_0}{L_s}\int_0^t [\varepsilon_i(t) - \varepsilon_r(t) - \varepsilon_t(t)]dt \tag{3}$$

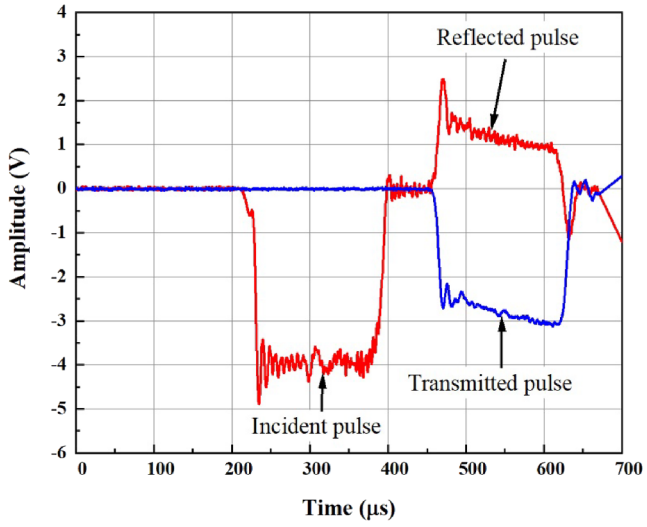


**Fig. 2.** Incident pulse, transmitted pulse and reflected pulse.

$$\dot{\varepsilon}(t) = \frac{c_0}{L_s}[\varepsilon_i(t) - \varepsilon_r(t) - \varepsilon_t(t)] \tag{4}$$

where $A$, $E$, are cross-sectional area and Young's modulus of the pressure bar, respectively; And $c_0$ is the elastic wave velocity in the pressure bar; $A_s$ and $L_s$ are the cross-sectional area and the length of the specimen.

By substituting Eq. (1) into the Eq. (2)–(4), the expressions can be written as

$$\sigma(t) = \frac{EA}{A_s}\varepsilon_t(t) \tag{5}$$

$$\varepsilon(t) = -\frac{2c_0}{L_s}\int_0^t \varepsilon_r(t)dt \tag{6}$$

$$\dot{\varepsilon}(t) = -\frac{2c_0}{L_s}\varepsilon_r(t) \tag{7}$$

### 2.2. Johnson-Cook model

The constitutive equations are usually applied to predict the dynamic behavior of material which include physically based constitutive models, phenomenological constitutive models and artificial neural network based modelling. The phenomenological constitutive models can be determined by fitting and regression analysis from the experimental data. Hence, these models are more preferred than physically based models to predict the dynamic behavior of materials over wide range of temperatures and strain rates since they can be integrated into finite element codes easily [12].

The Johnson-Cook constitutive equation, in which the influences of strains, strain rates and temperatures on the flow stress of the material was considered, is the most widely used phenomenological constitutive model to predict the dynamic behavior of material [10]. It was defined as

$$\sigma = (A + B\varepsilon^n)(1 + C\ln\dot{\varepsilon}^*)(1 - (T^*)^m) \tag{8}$$

where σ refers to the Von Misses flow stress, $\varepsilon$ is the equivalent plastic strain, $\dot{\varepsilon}^* = \dot{\varepsilon}/\dot{\varepsilon}_0$ is the dimensionless strain rate with $\dot{\varepsilon}^*$ and $\dot{\varepsilon}_0$ being the strain rate and the reference strain rate, respectively. $A$ is the yield stress at the reference temperature and reference strain rate; $B$ and $n$ are the coefficients of strain hardening; $C$ and $m$ are the material constants which represent the coefficients of strain rate hardening and thermal softening exponent. $T^*$ is dimensionless temperature and defined as

$$T^* = \frac{T - T_r}{T_m - T_r} \tag{9}$$

where $T$, $T_r$ and $T_m$ are the current absolute temperature, the reference

**Table 1**
Chemical compositions of the CuCrZr alloy.

| Alloy | Base alloying elements and impurities (wt. %) | | | |
|---|---|---|---|---|
| | Cu | Cr | Zr | Impurities |
| CuCrZr | base | 0.6–0.9 | 0.07–0.15 | Total < 0.1<br>Including Co < 0.05<br>O – as low as possible |

temperature (room temperature) and melting temperature.

The terms of $(A + B\varepsilon^n)$, $(1 + C\ln\dot{\varepsilon}^*)$ and $(1 - (T^*)^m)$ in Eq. (8) describe the effects of strain hardening, strain rate hardening and temperature softening of the metallic materials, respectively.

## 3. Experimental

The CuCrZr alloy used in this study was produced at Advanced Technology & Materials Co., Ltd. (AT&M). The chemical compositions of the CuCrZr alloy is within the range of ITER grade specification [13], as shown in Table 1.

A quasi-static compression test with a strain rate of 0.001 $s^{-1}$ was carried out to acquire basic stress–strain relationship by using an MTS hydro-servo system at room temperature (20 °C). And the dynamic tests were conducted by using a SHPB system. The shape and the size of the specimens are cylinders with dimensions of Φ 10 × 10 mm for quasi-static compression and cylinders with dimensions of Φ 8 × 8 mm, Φ 10 × 10 mm and Φ 12 × 12 mm for dynamic tests.

The tests were conducted over wide range of strain rates (500 ~ 2200 $s^{-1}$) and temperatures (20–600 °C). It would cover the whole range of strain rate and temperature which may need to concern for the CuCrZr alloy in the fusion device.

## 4. Result and discussion

### 4.1. Strain hardening

The stress–strain curve of quasi-static compression test is shown in Fig. 3. According to the data, the yield stress could be estimated by the crossing point of extended lines for the elastic and plastic stages of the curve [14]. It is about 235 MPa for this case, as shown in Fig. 3. Then, the effective stress–strain curve for the Johnson-Cook model could be obtained by subtracting the portion before the yield stress point of the true stress–strain curve since ε in the Johnson-Cook constitutive equation is equivalent plastic strain.

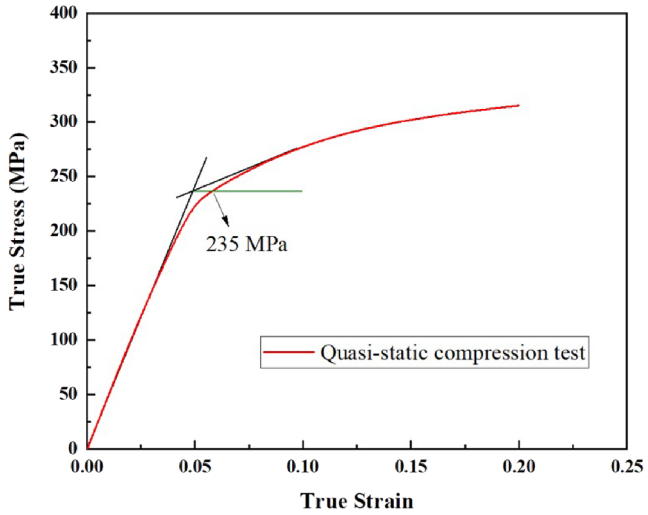


**Fig. 3.** The true stress–strain curves of CuCrZr of quasi-static compression test.

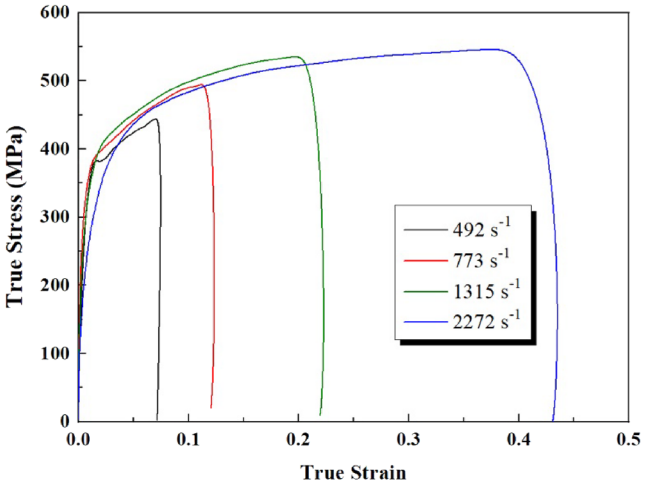


**Fig. 4.** The true stress–strain curves of CuCrZr for different strain rates at room temperature.

### 4.2. Strain rate hardening

The stress–strain curves of the CuCrZr alloy for different strain rates at room temperature are shown in Fig. 4. It can be found that the flow stress increases with the increase of strain rate at the same strain except at the strain rate of 2272 $s^{-1}$. This is the typical characteristic of dynamic behavior of materials, which is usually referred to as strain rate hardening effect. The abnormal mechanical behavior at the strain rate of 2272 $s^{-1}$ is attributed to the competition between the strain hardening and thermal softening as a result of adiabatic temperature rise with increasing the strain rate, especially in high strain rate deformation [12]. Furthermore, it can be found that the CuCrZr offers higher ductility in high strain rate deformation area which leads to that the onset of nonlinearity starts earlier in the case of strain rate of 2272 $s^{-1}$.

Based on the stress–strain curves, the yield stress of CuCrZr alloy for different strain rates at room temperature could be estimated, as summarized in Table 2. The yield stress increases from 359 MPa to 428 MPa when the strain rate improves from 492 $s^{-1}$ to 2272 $s^{-1}$. The result indicates that the CuCrZr alloy specimen exhibit a trend of strain rate hardening.

### 4.3. Thermal softening

Thermal softening is another important effect that needs to be considered in the dynamic behavior of the materials. The stress–strain curves of the CuCrZr alloy for different temperatures at strain rate about 2200 $s^{-1}$ are shown in Fig. 5.

It is obvious that the flow stress drops with the temperature increases at the same strain when the strain rate keeps constant. When the temperature increase, it will induce: 1) the thermal activation energy of the material increases; 2) the strength of obstacles decreases since thermal activation aids dislocation gliding; 3) the applied stress required to force the dislocation past obstacles reduces, which decreasing the flow stress [15].

According to the experiment results, the yield stress of CuCrZr alloy for different temperatures at strain rate about 2200 $s^{-1}$ could be estimated, as summarized in Table 3. The yield stress decreases from 428 MPa to 328 MPa when the temperature improves from 20 °C to

**Table 2**
Yield stress of CuCrZr for different strain rates at room temperature.

| Strain rate ($s^{-1}$) | 0.001 | 492 | 773 | 1315 | 2272 |
|---|---|---|---|---|---|
| Yield stress (MPa) | 235 | 359 | 372 | 397 | 428 |

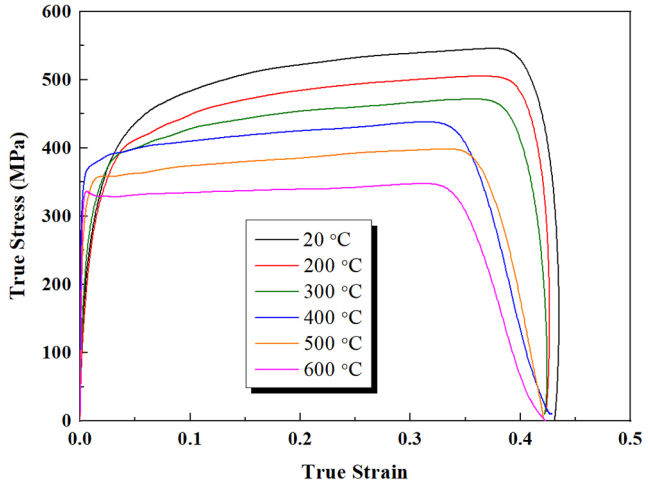


**Fig. 5.** The true stress–strain curves of CuCrZr for different temperatures at strain rate about 2200 $s^{-1}$.

**Table 3**
Yield stress of CuCrZr for different temperatures at strain rate about 2200 $s^{-1}$.

| Temperature (°C) | 20 | 200 | 300 | 400 | 500 | 600 |
|---|---|---|---|---|---|---|
| Yield stress (MPa) | 428 | 411 | 400 | 388 | 360 | 328 |

600 °C. Comparing with the results of strain rate hardening, the CuCrZr alloy specimen displays a distinct thermal softening effect.

## 5. Johnson-Cook constitutive equation

### 5.1. Johnson-Cook model

As aforementioned, the Johnson-cook model has five material constants which need to be determined by the experimental data. Considering that the three terms in the constitutive equation indicate the effects of strain hardening, strain rate hardening and temperature softening respectively, the parameters can be calculated step by step based on the experiment results above.

#### 5.1.1. Determination of material constants for strain hardening effect

According to the conditions in the quasi-static compression test, the reference strain rate and reference temperature are 0.001 $s^{-1}$ and 20 °C, respectively. The melting temperature for CuCrZr alloy is about 1080 °C. When these values are substituted into Eq. (8), only the term of strain hardening effect remains:

$$\sigma = A + B\varepsilon^n \tag{10}$$

The value of constant A could be obtained from the yield stress of the flow curve for the quasi-static compression test, $A = 235$ MPa. Taking natural logarithm of Eq. (10), it can be rewritten as:

$$\ln(\sigma - A) = \ln B + n \ln \varepsilon \tag{11}$$

Then substituting the value of $A$, the relationship between $\ln(\sigma - A)$ and $\ln \varepsilon$ could be given based on the experimental data, as shown in Fig. 6. The values of constant $B$ and $n$ could be obtained from the intercept and slope of the fitting line, namely, $B = 340$ and $n = 0.708$.

#### 5.1.2. Determination of material constants for strain rate hardening effect

In the experiments at room temperature, there is no thermal softening effect since $T^*$equals to 0. Then Eq. (8) can be described as:

$$\frac{\sigma}{A + B\varepsilon^n} = 1 + C \ln \dot{\varepsilon}^* \tag{12}$$

The value of $C$ could be obtained from the slope of $\sigma/(A + B\varepsilon^n)$ vs. $\ln \dot{\varepsilon}^*$ plot. According to the experimental data, the relationship could be evaluated by selecting series of strain (0.01–0.16). Then, the constant $C$ could be evaluated by the averaged fitting line, i.e. $C = 0.0474$, as shown in Fig. 7.

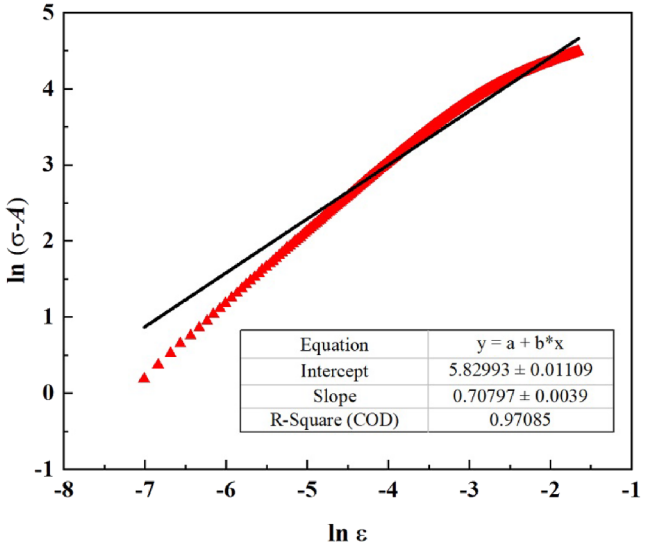


**Fig. 6.** The relationship between $\ln(\sigma - A)$ and $\ln \varepsilon$.

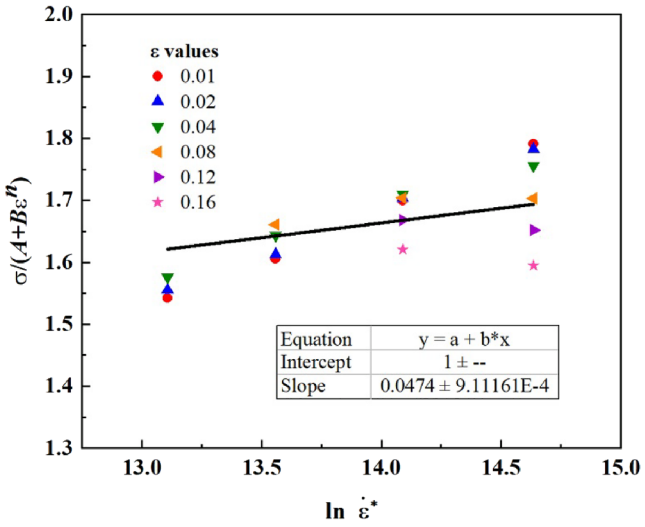


**Fig. 7.** The relationship between$\sigma/(A + B\varepsilon^n)$ and $\ln \dot{\varepsilon}^*$.

#### 5.1.3. Determination of material constants for thermal softening effect

To determine the constant $m$ in the Johnson-Cook constitutive equation, the Eq. (8) can be expressed as:

$$\ln\left[1 - \frac{\sigma}{(A + B\varepsilon^n)(1 + C \ln \dot{\varepsilon}^*)}\right] = m \ln T^* \tag{13}$$

Similarly, substituting the different temperatures and corresponding flow stress at different strain levels into Eq. (13), the relationship between $\ln(1 - (\sigma/(A + B\varepsilon^n)(1 + C \ln \dot{\varepsilon}^*)))$ and $\ln T^*$ could be obtained, as shown in Fig. 8. Then, the average value, $m = 1.831$, could be evaluated by linear fitting method.

#### 5.1.4. Comparisons between the experimental and predicted flow stress

In conclusion, the original Johnson-Cook constitutive equation for the CuCrZr alloy was established as:

$$\sigma = (235 + 340\varepsilon^{0.708})(1 + 0.0474 \ln \dot{\varepsilon}^*)(1 - (T^*)^{1.831}) \tag{14}$$

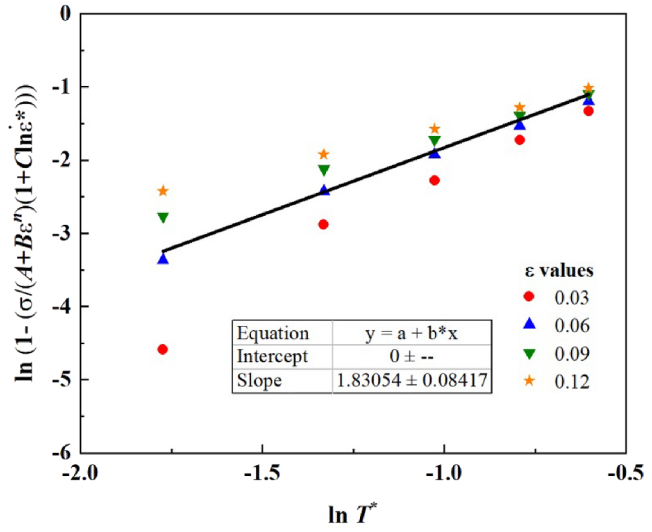


**Fig. 8.** The relationship between $\ln(1 - (\sigma/(A + B\varepsilon^n)(1 + C\ln\dot{\varepsilon}^*)))$ and $\ln T^*$

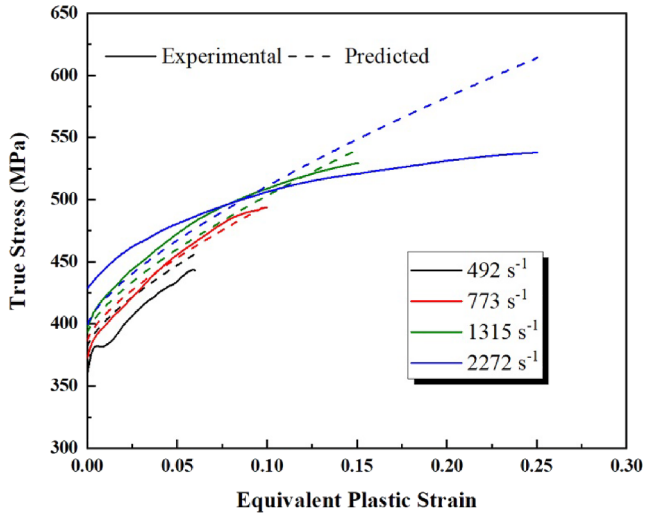


**Fig. 9.** Comparison between experimental and predicted flow stress by original Johnson-Cook model for different strain rates at room temperature

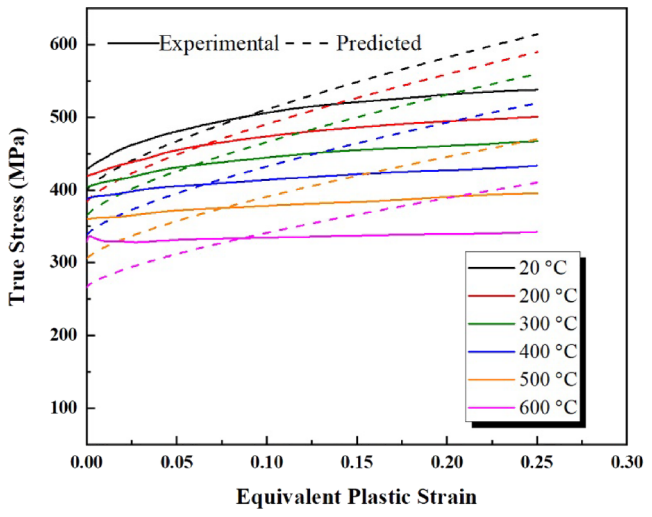


**Fig. 10.** Comparison between experimental and predicted flow stress by original Johnson-Cook model for different temperatures at strain rate about 2200 $s^{-1}$.

The comparisons between the experimental and predicted flow stress by Eq. (14) are shown in Fig. 9 and Fig. 10. It is obvious that the prediction by original Johnson-Cook model could not match well with the experimental data at high strain rate. Especially, the prediction at the strain rate 2272 $s^{-1}$ could not correctly reflect the flow behavior of the CuCrZr alloy. Although the inaccuracy at high strain rate will affects the reliability of the results in Fig. 10, it still can be found that the error of the predictions increases when the testing temperature increases. And the difference between the experimental and predicted flow stress changes when the strain increasing. All of these results are due to the original Johnson-Cook model assumes that the strain hardening, strain rate hardening and thermal softening are three independent phenomena and can be isolated from each other for the materials. Actually, the coupled effects of strain, strain rate and temperature could not be ignored [16].

### 5.2. Modified Johnson-Cook model

As depicted in Fig. 9, there is a huge variation between the predicted and experimental results when the strain rate goes to high strain rate region. A modified Johnson-Cook model was proposed in this study when considering the coupled effects of strain, strain rate and temperature on the behavior of material, which can describe the dynamic behaviors of the CuCrZr alloy accurately.

#### 5.2.1. Term of strain rate hardening

In the previous calculation for the original Johnson-Cook model, $C$ is the average value of strain rate hardening constant at different strain rates, which makes the predicted results inconsistent with the experimental data. An equation to consider the effects of both strains and strain rates on the strain rate hardening coefficient was proposed in the modified Johnson-Cook model, which can be expressed as follows [12]:

$$C(\varepsilon, \ln\dot{\varepsilon}^*) = C_0 + C_1\varepsilon + C_2\varepsilon^2 + C_3\varepsilon\ln\dot{\varepsilon}^* + C_4\ln\dot{\varepsilon}^* + C_5(\ln\dot{\varepsilon}^*)^2 \quad (15)$$

where $C_0$, $C_1$, $C_2$, $C_3$, $C_4$ and $C_5$ are the regression coefficients determined through the optimum regression methods. Based on the experimental data of different strain rates at room temperature, the values of these coefficients could be calculated, as summarized in Table 4.

#### 5.2.2. Term of thermal softening

The following equation was proposed to improve the terms of effect for thermal softening:

$$f(\varepsilon, T^*) = 1 - m_0(T^*)^{(m_1+m_2\varepsilon)} \quad (16)$$

Since the terms of strain hardening and strain rate hardening in the modified Johnson-Cook model had been determined, the coefficients of $m_0$, $m_1$ and $m_2$ could be calculated based on the experimental data by using the method described in section 5.1.3. The values of these coefficients are listed in Table 5.

#### 5.2.3. Verification of modified Johnson-Cook model

Considering all the parameters had been established, the modified Johnson-Cook model was expressed as:

$$\sigma = (235 + 340\varepsilon^{0.708})(1 + C(\varepsilon, \ln\dot{\varepsilon}^*)\ln\dot{\varepsilon}^*)(1 - 0.8(T^*)^{(1.5557-0.8639\varepsilon)}) \quad (17)$$

The comparisons between the experimental and predicted flow stress by Eq. (17) are shown in Fig. 11 and Fig. 12. It can be seen that the predicted flow stress is in good agreement with the experimental data.

**Table 4**
The values of coefficients for term of strain rate hardening.

| Coefficient | $C_0$ | $C_1$ | $C_2$ | $C_3$ | $C_4$ | $C_5$ |
|---|---|---|---|---|---|---|
| Value | −0.2697 | 1.4887 | −0.0556 | −0.1070 | 0.0368 | −0.0010 |

**Table 5**
The values of coefficients for term of thermal softening.

| Coefficient | $m_0$ | $m_1$ | $m_2$ |
|---|---|---|---|
| Value | 0.8 | 1.5557 | −0.8639 |

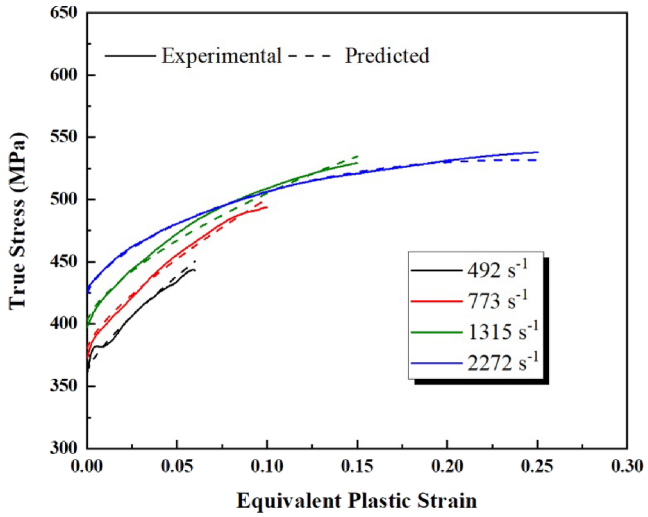


**Fig. 11.** Comparisons between experimental and predicted flow stress by modified Johnson-Cook model for different strain rates at room temperature.

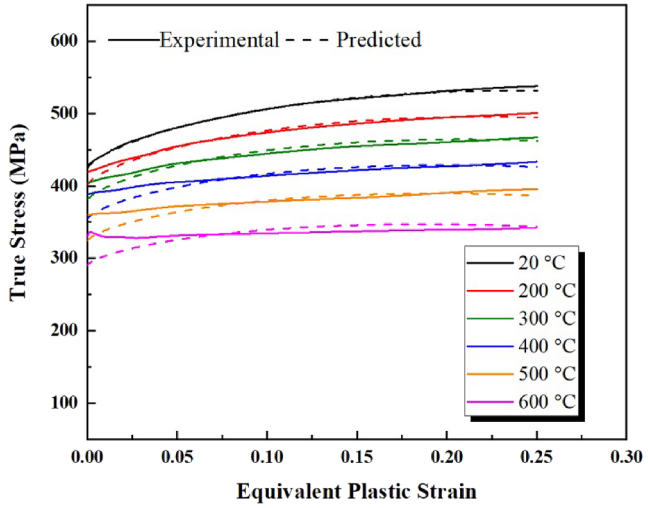


**Fig. 12.** Comparisons between experimental and predicted flow stress by modified Johnson-Cook model for different temperatures at strain rate about 2200 $s^{-1}$.

To further verify the reliability and predictability of modified Johnson-Cook model, the standard statistical parameters such as average absolute relative error (AARE) and root mean square error (RMSE) was calculated. The expressions are as follows:

$$AARE(\%) = \frac{1}{N}\sum_{i=1}^{N}\left|\frac{E_i - P_i}{E_i}\right| \times 100 \tag{18}$$

$$RMSE = \sqrt{\frac{1}{N}\sum_{i=1}^{N}(P_i - E_i)^2} \tag{19}$$

where $P_i$ is the predicted value by the model and $E_i$ is the corresponding experimental data. $N$ is the total number of the data.

The values of AARE and RMSE for original and modified Johnson-Cook model were summarized in Table 6 and Table 7 respectively. The

**Table 6**
AARE and RSME of original Johnson-Cook model (OJCM) and modified Johnson-Cook (MJCM) model for different strain rates at room temperature.

| Strain rate ($s^{-1}$) | 492 | 773 | 1315 | 2272 |
|---|---|---|---|---|
| OJCM_AARE (%) | 3.48 | 0.97 | 1.73 | 5.56 |
| MJCM_AARE (%) | 0.59 | 0.62 | 0.78 | 0.24 |
| OJCM_RMSE | 14.54 | 5.01 | 9.22 | 35.74 |
| MJCM_RMSE | 3.26 | 3.05 | 4.47 | 1.95 |

**Table 7**
AARE and RSME of original Johnson-Cook model (OJCM) and modified Johnson-Cook (MJCM) model for different temperatures at strain rate about 2200 $s^{-1}$.

| Temperature (°C) | 200 | 300 | 400 | 500 | 600 |
|---|---|---|---|---|---|
| OJCM_AARE (%) | 7.41 | 8.71 | 9.18 | 8.78 | 10.22 |
| MJCM_AARE (%) | 0.59 | 1.05 | 1.44 | 1.63 | 3.22 |
| OJCM_RMSE | 44.53 | 48.13 | 45.79 | 39.51 | 39.79 |
| MJCM_RMSE | 3.57 | 5.68 | 8.72 | 8.97 | 14.99 |

results indicate that deviation between predicted values by modified Johnson-Cook model and experimental data were much smaller than that of original Johnson-Cook model. Combination with Fig. 11 and Fig. 12, it implied that the modified Johnson-Cook model can give an accurate and credible estimate of the flow stress for CuCrZr alloy over wide range of strain rates and temperatures.

## 6. Conclusions

In this work, the dynamic compressive characteristics of CuCrZr alloy had been studied by SHPB technique over practical range of strain rates and temperatures. The experimental stress–strain curves indicated that the CuCrZr alloy has the typical characteristics of strain rate hardening and temperature softening effect.

Afterwards, the constitutive equation was established to predict the dynamic behavior of CuCrZr alloy based on Johnson-Cook model. With a detailed study of the comparison between the predicted results by Johnson-Cook model and experimental data in all situations, a modified Johnson-Cook model to consider the coupled effects of strain, strain rate and temperature on the behavior of material had been proposed in order to present an accurate and credible estimate of the dynamic behavior of CuCrZr alloy. A remarkable accordance between the results from the modified Johnson-Cook model and from experimental data under all conditions was observed, which means that the modified Johnson-Cook model can give an accurate and credible prediction of the dynamic behavior for CuCrZr alloy over wide range of strain rates and temperatures. The developed constitutive equation would be helpful to study the dynamic response of CuCrZr alloy in the ITER and fusion devices.

## CRediT authorship contribution statement

**Xinyuan Qian:** Conceptualization, Methodology, Formal analysis, Writing - original draft, Writing - review & editing. **Xuebing Peng:** Methodology, Project administration, Funding acquisition. **Yuntao Song:** Conceptualization, Supervision. **Jianjun Huang:** Supervision. **Yanpeng Wei:** Investigation, Resources. **Peng Liu:** Data curation, Visualization. **Xin Mao:** Validation. **Jianwu Zhang:** Formal analysis. **Liang Wang:** Supervision.

## Declaration of Competing Interest

The authors declare that they have no known competing financial interests or personal relationships that could have appeared to influence the work reported in this paper.

## Acknowledgements

This work was supported by National Natural Science Foundation of China No. 11705234 and International Partnership Program of Chinese Academy of Sciences No. Y16YZ17271. And we also would like to acknowledge the support of Shenzhen Clean Energy Research Institute.

## References

[1] T. Hirai, V. Barabash, F. Escourbiac, A. Durocher, L. Ferrand, V. Komarov, M. Merola, ITER divertor materials and manufacturing challenges, Fusion Eng. Des. 125 (2017) 250–255, https://doi.org/10.1016/j.fusengdes.2017.07.009.

[2] S. Qin, D. Yao, Q. Wang, X. Mao, P. Liu, X. Qian, T. Xu, L. Li, X. Peng, K. Lu, Y. Song, Preliminary design progress of the CFETR water-cooled divertor, IEEE Trans. Plasma Sci. 48 (2020) 1–10, https://doi.org/10.1109/tps.2020.2985735.

[3] G. Pintsuk, E. Diegele, S.L. Dudarev, M. Gorley, J. Henry, J. Reiser, M. Rieth, European materials development: results and perspective, Fusion Eng. Des. 146 (2019) 1300–1307, https://doi.org/10.1016/j.fusengdes.2019.02.063.

[4] K. Tobita, R. Hiwatari, Y. Sakamoto, Y. Someya, N. Asakura, H. Utoh, Y. Miyoshi, S. Tokunaga, Y. Homma, S. Kakudate, N. Nakajima, Japan's efforts to develop the concept of JA DEMO during the past decade, Fusion Sci. Technol. 75 (2019) 372–383, https://doi.org/10.1080/15361055.2019.1600931.

[5] S. Kwon, K. Im, S.H. Hong, H. Lee, T.D. Rognlien, W. Meyer, K. Kim, Recent progress in the design of the K-DEMO divertor, Fusion Eng. Des. 159 (2020) 111770, , https://doi.org/10.1016/j.fusengdes.2020.111770.

[6] G.-N. Luo, G.H. Liu, Q. Li, S.G. Qin, W.J. Wang, Y.L. Shi, C.Y. Xie, Z.M. Chen, M. Missirlian, D. Guilhem, M. Richou, T. Hirai, F. Escourbiac, D.M. Yao, J.L. Chen, T.J. Wang, J. Bucalossi, M. Merola, J.G. LiEAST TEAM, Overview of decade-long development of plasma-facing components at ASIPP, Nucl. Fusion 57 (2017) 065001, , https://doi.org/10.1088/1741-4326/aa6502.

[7] M. Lipa, A. Durocher, R. Tivey, T. Huber, B. Schedler, J. Weigert, The use of copper alloy CuCrZr as a structural material for actively cooled plasma facing and in vessel components, Fusion Eng. Des. 75–79 (2005) 469–473, https://doi.org/10.1016/j.fusengdes.2005.06.056.

[8] J. Boscary, G. Ehrke, H. Greuner, P. Junghanns, C. Li, B. Mendelevitch, J. Springer, R. Stadlerthe W7-X Team, Progress in the production of the W7-X divertor target modules, Fusion Eng. Des. 146 (2019) 1975–1978, https://doi.org/10.1016/j.fusengdes.2019.03.080.

[9] C.C. Zhu, Y.T. Song, X.B. Peng, Y.P. Wei, X. Mao, W.X. Li, X.Y. Qian, The dynamical mechanical properties of tungsten under compression at working temperature range of divertors, J. Nucl. Mater. 469 (2016) 120–124, https://doi.org/10.1016/j.jnucmat.2015.11.045.

[10] G.R. Johnson, W.H. Cook, Fracture characteristics of three metals subjected to various strains, strain rates, temperatures and pressures, Eng. Fract. Mech. 21 (1985) 31–48, https://doi.org/10.1016/0013-7944(85)90052-9.

[11] J.E. Field, S.M. Walley, W.G. Proud, H.T. Goldrein, C.R. Siviour, Review of experimental techniques for high rate deformation and shock studies, Int. J. Impact Eng. 30 (2004) 725–775, https://doi.org/10.1016/j.ijimpeng.2004.03.005.

[12] A. Abd El-Aty, Y. Xu, S.H. Zhang, S. Ha, Y. Ma, D. Chen, Impact of high strain rate deformation on the mechanical behavior, fracture mechanisms and anisotropic response of 2060 Al-Cu-Li alloy, J. Adv. Res. 18 (2019) 19–37, https://doi.org/10.1016/j.jare.2019.01.012.

[13] V.R. Barabash, G.M. Kalinin, S.A. Fabritsiev, S.J. Zinkle, Specification of CuCrZr alloy properties after various thermo-mechanical treatments and design allowables including neutron irradiation effects, J. Nucl. Mater. 417 (2011) 904–907, https://doi.org/10.1016/j.jnucmat.2010.12.158.

[14] M. Dinkgreve, J. Paredes, M.M. Denn, D. Bonn, On different ways of measuring "the" yield stress, J. Nonnewton. Fluid Mech. 238 (2016) 233–241, https://doi.org/10.1016/j.jnnfm.2016.11.001.

[15] A. Rusinek, J.A. Rodríguez-Martínez, A. Arias, A thermo-viscoplastic constitutive model for FCC metals with application to OFHC copper, Int. J. Mech. Sci. 52 (2010) 120–135, https://doi.org/10.1016/j.ijmecsci.2009.07.001.

[16] Y.C. Lin, X. Chen, G. Liu, A modified Johnson – Cook model for tensile behaviors of typical high-strength alloy steel, Mater. Sci. Eng., A 527 (2010) 6980–6986, https://doi.org/10.1016/j.msea.2010.07.061.